LETTER

doi:10.1038/nature09418

Generation of three-qubit entangled states using superconducting phase qubits

Matthew Neeley[1], Radoslaw C. Bialczak[1], M. Lenander[1], E. Lucero[1], Matteo Mariantoni[1], A. D. O'Connell[1], D. Sank[1], H. Wang[1], M. Weides[1], J. Wenner[1], Y. Yin[1], T. Yamamoto[1,2], A. N. Cleland[1] & John M. Martinis[1]

Entanglement is one of the key resources required for quantum computation[1], so the experimental creation and measurement of entangled states is of crucial importance for various physical implementations of quantum computers[2]. In superconducting devices[3], two-qubit entangled states have been demonstrated and used to show violations of Bell's inequality[4] and to implement simple quantum algorithms[5]. Unlike the two-qubit case, where all maximally entangled two-qubit states are equivalent up to local changes of basis, three qubits can be entangled in two fundamentally different ways[6]. These are typified by the states $|GHZ\rangle = (|000\rangle + |111\rangle)/\sqrt{2}$ and $|W\rangle = (|001\rangle + |010\rangle + |100\rangle)/\sqrt{3}$. Here we demonstrate the operation of three coupled superconducting phase qubits[7] and use them to create and measure $|GHZ\rangle$ and $|W\rangle$ states. The states are fully characterized using quantum state tomography[8] and are shown to satisfy entanglement witnesses[9], confirming that they are indeed examples of three-qubit entanglement and are not separable into mixtures of two-qubit entanglement.

To create arbitrary entangled states or perform arbitrary computations, a quantum computer must implement a set of universal gates[1], typically taken to be a two-qubit gate such as controlled-NOT (CNOT) plus single-qubit rotations[10]. Alternatively, universality is possible using a three-qubit gate such as the Toffoli gate[11–13]. Three-qubit gates are also important in such applications as quantum error correction[14], and they can simplify some quantum circuits[12]. Because superconducting phase qubits can be coupled simply by connecting them with a capacitor[7], we can design multi-qubit interactions that directly generate multi-qubit gates[15], rather than building them up from more elementary two-qubit gates. To create the two types of three-qubit entanglement we take both approaches, using two-qubit gates for the $|GHZ\rangle$ protocol and a more efficient entangling protocol, based on a single three-qubit gate, for the $|W\rangle$ protocol. Independent work in which three-qubit entanglement is created using coupled transmon qubits is reported in a companion publication[16].

Our $|GHZ\rangle$ protocol[17,18] is shown as a quantum circuit diagram in Fig. 1a. Starting in the ground state, $|000\rangle$, a rotation is applied to qubit A to create the superposition $(|000\rangle + |100\rangle)/\sqrt{2}$. Next, a CNOT gate is applied to flip qubit B conditioned on qubit A, resulting in the state $(|000\rangle + |110\rangle)/\sqrt{2}$. Finally, a second CNOT gate is applied to flip qubit C conditioned on B, resulting in the desired state, $|GHZ\rangle$. As is typical with quantum circuits, this is written in terms of CNOT gates, which take a simple form in the qubit basis. In our system, a more natural universal gate is the iSWAP gate[19], by which $|01\rangle \rightarrow -i|10\rangle$ and $|10\rangle \rightarrow -i|01\rangle$, with $|00\rangle$ and $|11\rangle$ unchanged. This gate is generated by applying the available coupling interaction, $H_{int}^{AB} = (\hbar g/2)(\sigma_x^A\sigma_x^B + \sigma_y^A\sigma_y^B)$, for time $t_{iSWAP} = \pi/2g$, where g is the coupling strength, $\hbar$ is Planck's constant divided by 2π and the σs are Pauli X and Y operators on qubits A and B. The $|GHZ\rangle$ protocol can be 'recompiled' in terms of this gate to obtain the circuit shown in Fig. 1b.

The protocol to generate a $|W\rangle$ state (Fig. 1c) is based on two features of the state: it is symmetric with respect to permutations of the qubits and it is a superposition of three states in each of which one qubit is excited. Thus, generating the state requires 'sharing' a single excitation symmetrically among three qubits. This is done by first applying a π-pulse to qubit B to excite it with one photon and create the state $|010\rangle$. Then the qubits are entangled by turning on an equal interaction between all pairs, $H_{int} = H_{int}^{AB} + H_{int}^{AC} + H_{int}^{BC}$, for time $t_W = (4/9)t_{iSWAP}$. The interaction causes the excitation to be distributed among the qubits, and at time t_W the system is left in an equal superposition state, as desired. A final Pauli Z rotation can then be applied to correct the phase of qubit B, although this does not affect the entanglement of the state. This protocol requires only a single entangling operation, and the interaction is only applied for a short time, shorter even than the characteristic time for two-qubit gates in the system. This yields a highly efficient state-generation protocol based on the multi-qubit gate generated by H_{int}.

To allow for future expansion beyond the present work, the sample was designed with four qubits, such that the coupling network for the

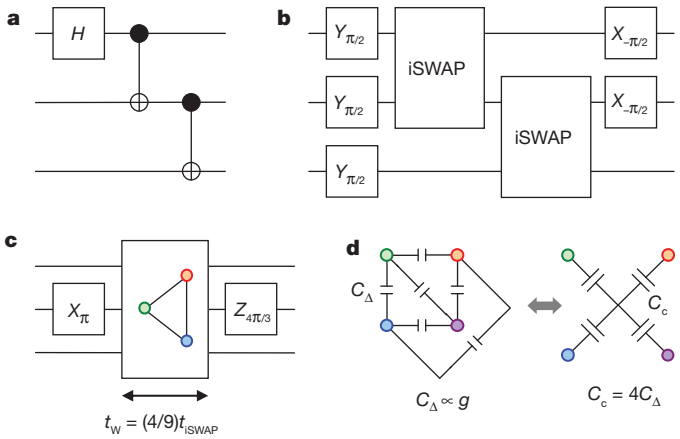

Figure 1 | Protocols for generating entangled states. a, Quantum circuit for generating $|GHZ\rangle$ using CNOT gates. **b**, Quantum circuit for $|GHZ\rangle$ that has been 'recompiled' to use iSWAP gates, which are directly generated by capacitive coupling in the phase qubit. These two circuits are not fully equivalent, but they both produce $|GHZ\rangle$ when operating on the ground state as input. **c**, Circuit to generate $|W\rangle$ using a single entangling step with simultaneous coupling between all three qubits. The entangling operation is turned on for a time $t_W = (4/9)t_{iSWAP}$, where t_{iSWAP} is the time needed to complete an iSWAP gate between two qubits. In these quantum circuits, H represents the Hadamard gate, and X, Y and Z are rotations about the respective axes of the Bloch sphere by the subscript angles[1]. **d**, Capacitive coupling network to achieve symmetric coupling between all pairs of qubits (left), and simplified equivalent circuit using coupling to a central island (right). The complete network on the left requires six capacitors, and the coupling strength, g, is proportional to the qubit–qubit capacitance, C_Δ. In the equivalent circuit on the right, the same coupling strength is attained by scaling the capacitors to $C_c = 4C_\Delta$, but now only four capacitors are required and the circuit can be easily laid out symmetrically on a chip.

[1]Department of Physics, University of California, Santa Barbara, California 93106, USA. [2]Green Innovation Research Laboratories, NEC Corporation, Tsukuba, Ibaraki 305-8501, Japan.

desired symmetric coupling between all pairs of qubits is as shown on the left in Fig. 1d. The design can be simplified by transforming the coupling network into an equivalent circuit (Fig. 1d, right) in which each qubit is coupled capacitively to a central 'island' (Supplementary Information). This simplified design is easier to lay out symmetrically on chip and requires only N capacitors to couple N qubits, rather than the $N(N-1)/2$ capacitors in the complete network.

Figure 2a shows the complete schematic of the device with four phase qubits connected by the capacitive island coupler. Each qubit is individually controlled by a bias coil that sets the operating flux bias and carries microwave pulses for manipulating and measuring the qubit state. In addition, each qubit is coupled to an on-chip SQUID for state read-out. Figure 2b shows a micrograph of the fabricated device, made from aluminium films on sapphire substrate with Al–AlO_x–Al Josephson junctions. The completed device is mounted in a superconducting aluminium sample holder and cooled in a dilution refrigerator to ~25 mK. Initial calibration of the multi-qubit device is similar to that described in previous works[20,21]. Although the coupling capacitors are fixed, the effective interaction can be controlled by tuning the qubits into resonance at $f_B = 6.55$ GHz (coupling 'on') or by detuning qubits A and C to ± 250 MHz (coupling off)[22]. The measured coupling strengths were found to be within 5% of 12.5 MHz for each pair of qubits. Notably, all qubits can be brought into resonance simultaneously, as required for the $|W\rangle$ protocol, or two qubits can be tuned into resonance with the third detuned, as required for the iSWAP gates in the $|GHZ\rangle$ protocol.

Capacitive coupling as used here is simple and well understood but is subject to measurement cross-talk[4,7], which can cause, for example, a state $|001\rangle$ to be erroneously read out as $|011\rangle$, $|101\rangle$ or even $|111\rangle$. This cross-talk affects measured probabilities of all excited-state populations; however, it has no effect on the 'null-result' probability of measuring $|000\rangle$, because cross-talk can only act if at least one qubit is excited. By measuring various subsets of qubits and recording the null-result probability for each subset, we are able to reconstruct the combined state occupation probabilities without any effect from measurement cross-talk (Supplementary Information).

Figure 3 shows the time evolution of the state occupation probabilities during for the entangling protocols, using cross-talk-free measurement. In the $|W\rangle$ protocol (Fig. 3a), one qubit is excited and then the symmetric interaction between all pairs of qubits is used to distribute that excitation among all three, as described above. When the interaction time is chosen properly, the system reaches an equal superposition and subsequently stays there while the interaction is off (Fig. 3b). Because this one excitation is swapped among the various qubits, the state evolution during this protocol is clearly visible in the occupation probabilities as they change

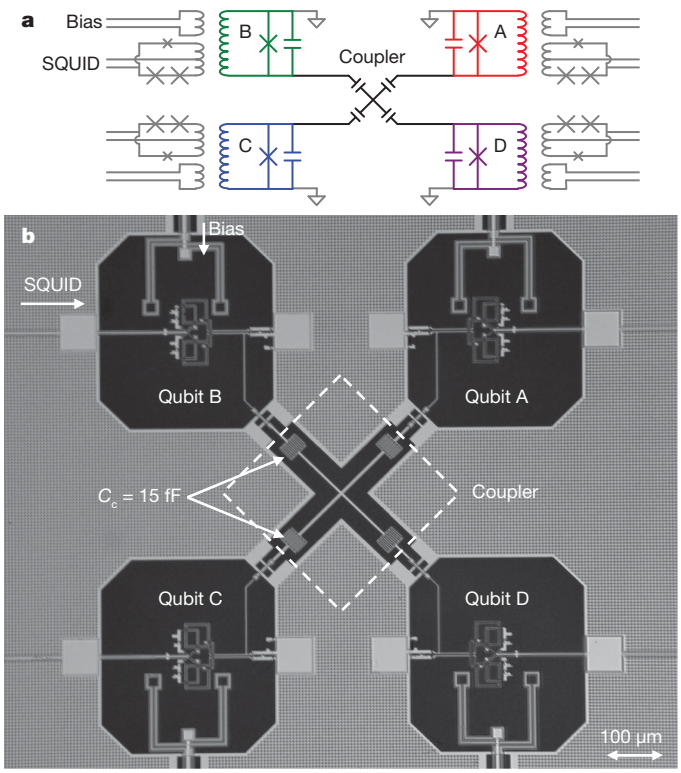

Figure 2 | Device description and operation. **a**, Schematic of coupled-qubit circuit. Each qubit is controlled individually by a flux bias line that sets the d.c. operating point, provides quasi-d.c. pulses for tuning the qubits in and out of resonance and provides a.c. (microwave) control signals for qubit rotations. In addition, each qubit is coupled to a superconducting quantum interference device (SQUID) for read-out of the qubit state. The qubits are capacitively coupled to the central island, which results in symmetric coupling between all pairs of qubits. **b**, Photomicrograph of the sample, fabricated with aluminium (light areas) on sapphire substrate (dark areas). The coupler is the cross-shaped structure in the centre, and the simplicity of this design is evident in the straightforward correspondence between the schematic and the completed device. The entire sample is mounted in a superconducting aluminium box and cooled to 25 mK in a dilution refrigerator.

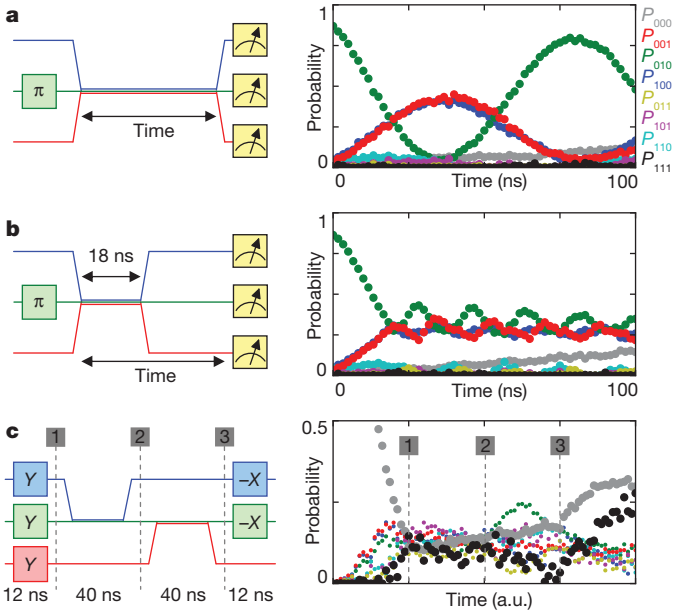

Figure 3 | Generation of entangled states in the time domain. In each panel, the pulse sequence is shown on the left with time on the horizontal axis and qubit frequency on the vertical axis, and the measured state occupation probabilities (P_{abc}) are shown on the right. **a**, To characterize the three-qubit interaction, all qubits are initially detuned and qubit B is excited with a π-pulse. The qubits are then tuned into resonance to interact for some time, then detuned and measured. During the interaction, the excitation from qubit B ($|010\rangle$) is swapped to qubits A and C ($|100\rangle$ and $|001\rangle$), and then back again. Owing to the coupling symmetry, P_{100} and P_{001} are nearly equal throughout the entire sequence. At the crossing point where the three probabilities are equal, the system is in a $|W\rangle$ state. **b**, The coupling is turned on until the crossing point is reached and then the qubits are detuned, leaving the system in a $|W\rangle$ state. The small oscillations visible thereafter are caused by residual coupling due to the finite detuning. **c**, The $|GHZ\rangle$ sequence is a translation of the circuit in Fig. 1b, with the iSWAP gates implemented by tuning the qubits pairwise into resonance for time $t_{iSWAP} = 40$ ns and π/2 rotations implemented by 12-ns microwave pulses for a total length of 104 ns. At right, the probabilities are plotted versus time in each marked stage of the sequence. After creating the initial superposition (1), the two iSWAP gates change the phases of the various components of the state, with little effect on the populations (1–2, 2–3). The final rotations populate $|000\rangle$ and $|111\rangle$ while depopulating the other states. For an ideal $|GHZ\rangle$ state, P_{000} and P_{111} should approach 50%, although in the experiment these levels are reduced owing to decoherence and errors, as discussed in the text. a.u., arbitrary units.

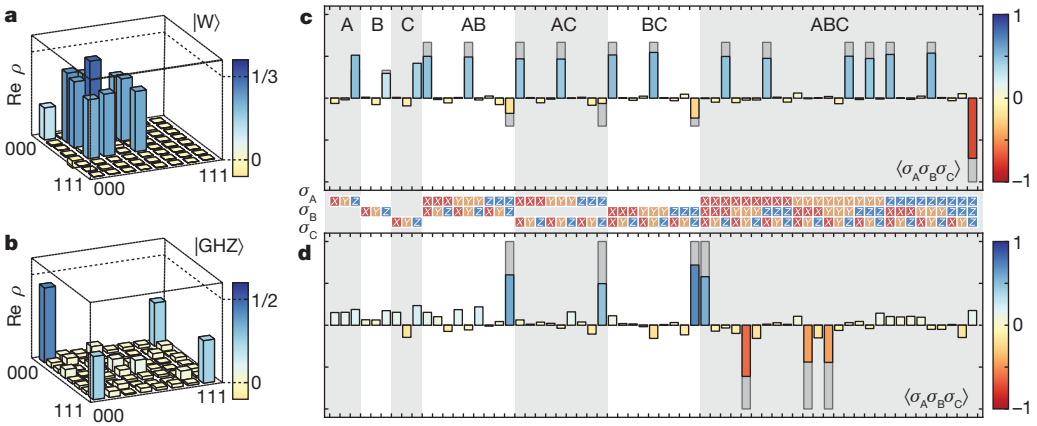

Figure 4 | Quantum state tomography of $|GHZ\rangle$ and $|W\rangle$. **a**, **b**, Real parts of the measured density matrices ρ_W (**a**) and ρ_{GHZ} (**b**). For both states, the theoretical density matrix has vanishing imaginary part, and the measured imaginary parts (not shown) are also found to be small, with $|\mathrm{Im}\,\rho_W| < 0.03$ and $|\mathrm{Im}\,\rho_{GHZ}| < 0.10$. **c**, **d**, Pauli set (generalized Stokes parameters) plotted for ρ_W (**c**) and ρ_{GHZ} (**d**). The bars show expectation values of combinations of Pauli operators on one, two and three qubits, with theory in grey and experiment overlaid in colour. The same state information is contained in both representations, but the Pauli sets clearly show the differences between $|W\rangle$-type and $|GHZ\rangle$-type entanglement. In addition to the three-qubit correlation terms, the $|W\rangle$ state has two-qubit correlations because tracing out one qubit from a $|W\rangle$ state leaves the others still partially entangled. The fidelity is $F_W = 0.78 \pm 0.01$. For $|GHZ\rangle$, the two-qubit correlations other than the trivial ZZ type are absent because tracing out one qubit leaves the others in a completely mixed state. The fidelity is $F_{GHZ} = 0.62 \pm 0.01$ and the state is also found to violate the Mermin–Bell inequality[23,24].

in time. The 5% asymmetry in coupling strengths leads to small errors that could be corrected by fine-tuning the interaction times, though this was not done here.

Figure 3c shows the state occupation probabilities during the $|GHZ\rangle$ protocol, plotted in segments corresponding to the stages of the protocol as indicated. The initial rotations create an equal superposition of all qubit states, with all probabilities converging on 1/8. The effect of the two iSWAP gates is then primarily to adjust the phases of the various components of the superpositions, such that in the final rotations $|000\rangle$ and $|111\rangle$ are populated and all other states are depopulated. The occupation probabilities behave as expected, but most of the state evolution is hidden in the phase information not captured by these probability measurements.

To fully characterize the quantum states created by the entangling protocols, including the phase information, we perform quantum state tomography by applying various combinations of single-qubit rotations before measurement. The density matrix is extracted from the measured data using maximum-likelihood estimation to find the state that best fits the data while also satisfying the physicality constraints that it be Hermitian, positive semi-definite and have unit trace. Using this procedure, we extract the density matrices ρ_W and ρ_{GHZ}, whose respective real parts are shown in Fig. 4a and Fig. 4b, and whose respective Pauli sets (expectation values of one-, two- and three-qubit Pauli operators) are shown in Fig. 4c and Fig. 4d. Comparing the measured states with theory, we find fidelities $F_W = \langle W|\rho_W|W\rangle = 0.78 \pm 0.01$ and $F_{GHZ} = \langle GHZ|\rho_{GHZ}|GHZ\rangle = 0.62 \pm 0.01$.

To understand the significance of the measured fidelities, we compare these results with entanglement witness operators that detect three-qubit entanglement. Three-qubit entanglement is witnessed[9] for the $|W\rangle$ state provided that $F_W > 2/3$, and for the $|GHZ\rangle$ state provided that $F_{GHZ} > 1/2$. These inequalities are satisfied by the respective measured density matrices, indicating that they are genuine three-qubit entangled states that cannot be decomposed into mixtures of separable states. In addition, we find that ρ_{GHZ} violates the Mermin–Bell inequality[23] $G \equiv \langle XXX\rangle - \langle XYY\rangle - \langle YXY\rangle - \langle YYX\rangle \leq 2$, as we measure a value of $G_{\rho_{GHZ}} = 2.076 \pm 0.029$, contradicting the classical assumptions of local reality (Supplementary Information). The violation is not free from loopholes, owing to use of the cross-talk-free measurement protocol rather than a simultaneous measurement protocol[4], but it is nonetheless an indicator of genuine three-qubit entanglement.

The lower fidelity of $|GHZ\rangle$ relative to $|W\rangle$ is due to two main factors. First, the $|GHZ\rangle$ sequence is longer because of the two iSWAP gates; the sequence length is a substantial fraction of the dephasing time of the qubits, T_2, which is particularly detrimental because the sequence relies on precise phases produced by the gates to populate $|000\rangle$ and $|111\rangle$ while depopulating all other states. Longer coherence times would improve this, as would stronger coupling to reduce the gate time. Second, the presence of $|2\rangle$, and higher levels, and the relatively small nonlinearity of the phase qubit cause errors due to transitions into higher excited states, for example $|110\rangle \rightarrow |200\rangle$. These transitions can be ignored in the $|W\rangle$ protocol because they are inaccessible with only one excitation in the system, but they cause errors in the $|GHZ\rangle$ protocol because all qubit states are populated, including those with multiple excitations. The effect of higher levels becomes particularly complicated in this experiment when using fixed capacitive coupling with detuning to turn off the interaction, owing to spectral crowding from the higher qubit levels. This highlights the need to replace frequency detuning with tunable coupling schemes, which are currently an active area of research.

The states that we have generated violate entanglement witnesses that rule out biseparability, showing genuine three-party entanglement. This ability to couple three qubits and create entangled states with qualitatively different types of entanglement is a significant step towards scalable quantum information processing with superconducting devices.

Received 20 April; accepted 11 August 2010.

1. Nielsen, M. A. & Chuang, I. L. *Quantum Computation and Quantum Information* (Cambridge Univ. Press, 2000).
2. Ladd, T. D. *et al.* Quantum computers. *Nature* **464,** 45–53 (2010).
3. Clarke, J. & Wilhelm, F. K. Superconducting quantum bits. *Nature* **453,** 1031–1042 (2008).
4. Ansmann, M. *et al.* Violation of Bell's inequality in Josephson phase qubits. *Nature* **461,** 504–506 (2009).
5. DiCarlo, L. *et al.* Demonstration of two-qubit algorithms with a superconducting quantum processor. *Nature* **460,** 240–244 (2009).
6. Dür, W., Vidal, G. & Cirac, J. I. Three qubits can be entangled in two inequivalent ways. *Phys. Rev. A* **62,** 062314 (2000).
7. McDermott, R. *et al.* Simultaneous state measurement of coupled Josephson phase qubits. *Science* **307,** 1299–1302 (2005).
8. Steffen, M. *et al.* Measurement of the entanglement of two superconducting qubits via state tomography. *Science* **313,** 1423–1425 (2006).
9. Acín, A., Bruss, D., Lewenstein, M. & Sanpera, A. Classification of mixed three-qubit states. *Phys. Rev. Lett.* **87,** 040401 (2001).
10. Barenco, A. *et al.* Elementary gates for quantum computation. *Phys. Rev. A* **52,** 3457–3467 (1995).
11. Shi, Y. Both Toffoli and controlled-NOT need little help to do universal quantum computation. *Quantum Inf. Comput.* **3,** 84–92 (2003).

12. Lanyon, B. P. *et al.* Simplifying quantum logic using higher-dimensional Hilbert spaces. *Nature Phys.* **5,** 134–140 (2008).
13. Monz, T. *et al.* Realization of the quantum Toffoli gate with trapped ions. *Phys. Rev. Lett.* **102,** 040501 (2009).
14. Cory, D. G. *et al.* Experimental quantum error correction. *Phys. Rev. Lett.* **81,** 2152–2155 (1998).
15. Galiautdinov, A. & Martinis, J. M. Maximally entangling tripartite protocols for Josephson phase qubits. *Phys. Rev. A* **78,** 010305 (2008).
16. DiCarlo, L. *et al.* Preparation and measurement of three-qubit entanglement in a superconducting circuit. *Nature* doi:10.1038/nature09416 (this issue).
17. Wei, L. F., Liu, Y. X. & Nori, F. Generation and control of Greenberger-Horne-Zeilinger entanglement in superconducting circuits. *Phys. Rev. Lett.* **96,** 246803 (2006).
18. Matsuo, S. *et al.* Generation of macroscopic entangled states in coupled superconducting phase qubits. *J. Phys. Soc. Jpn* **76,** 054802 (2007).
19. Schuch, N. & Siewert, J. Natural two-qubit gate for quantum computation using the XY interaction. *Phys. Rev. A* **67,** 032301 (2003).
20. Lucero, E. *et al.* High-fidelity gates in a single Josephson qubit. *Phys. Rev. Lett.* **100,** 247001 (2008).
21. Neeley, M. *et al.* Emulation of a quantum spin with a superconducting phase qudit. *Science* **325,** 722–725 (2009).
22. Hofheinz, M. *et al.* Synthesizing arbitrary quantum states in a superconducting resonator. *Nature* **459,** 546–549 (2009).
23. Mermin, N. D. Extreme quantum entanglement in a superposition of macroscopically distinct states. *Phys. Rev. Lett.* **65,** 1838–1840 (1990).
24. Pan, J.-W., Bouwmeester, D., Daniell, M., Weinfurter, H. & Zeilinger, A. Experimental test of quantum nonlocality in three-photon Greenberger–Horne–Zeilinger entanglement. *Nature* **403,** 515–519 (2000).

Supplementary Information is linked to the online version of the paper at www.nature.com/nature.

Acknowledgements Devices were made at the UCSB Nanofabrication Facility, a part of the NSF-funded National Nanotechnology Infrastructure Network. This work was supported by IARPA under grant W911NF-04-1-0204. M.M. acknowledges support from an Elings Fellowship.

Author Contributions M.N. fabricated the sample, performed the experiments and analysed the data. J.M.M. and E.L. designed the custom electronics. H.W. and T.Y. contributed to software infrastructure. All authors contributed to the fabrication process, qubit design, experimental set-up and manuscript preparation.

Author Information Reprints and permissions information is available at www.nature.com/reprints. The authors declare no competing financial interests. Readers are welcome to comment on the online version of this article at www.nature.com/nature. Correspondence and requests for materials should be addressed to J.M.M. (martinis@physics.ucsb.edu).